ACS APPLIED MATERIALS & INTERFACES

Research Article

www.acsami.org

In Situ EQCM Study Examining Irreversible Changes the Sulfur–Carbon Cathode in Lithium–Sulfur Batteries

Heng-Liang Wu, Laura A. Huff, Jennifer L. Esbenshade, and Andrew A. Gewirth*

Department of Chemistry, University of Illinois at Urbana–Champaign, 600 S. Mathews Avenue, Urbana, Illinois 61801, United States

Supporting Information

ABSTRACT: In situ EQCM experiments were used to investigate the stability and roughness changes occurring in a sulfur–carbon cathode utilized for a Li–S battery during the charge–discharge process. Results show that the sulfur–carbon cathode gains mass during the first discharge plateau (~2.4 V) due to the formation of the long chain polysulfides during the discharge (lithiation) process. However, further discharge to below 2.4 V yields an increase in the crystal resistance (R_c) suggesting the sulfur–carbon cathode becomes rougher. During the charge (delithiation) process, the roughness of the sulfur–carbon cathode decreases. Time dependent measurements show that the electrode surface becomes rougher with the deeper discharge, with the change occurring following a step to 1.5 V. The sulfur–carbon cathode exhibits stable R_c and frequency behavior initially, but then becomes rougher in subsequent following cycles.

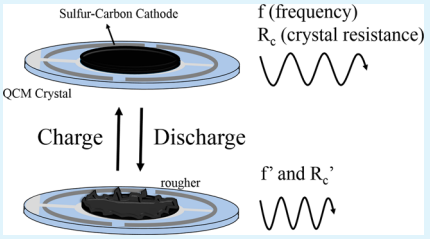

KEYWORDS: *Li–S batteries, EQCM, crystal resistance, polysulfide dissolution, roughness of the sulfur–carbon cathode*

1. INTRODUCTION

Li-ion batteries have dominated the consumer electronics market over the past few decades, especially in portable devices. However, their gravimetric and volumetric energy density is limited (typically around 400 Wh kg^{-1} and 1100 Wh L^{-1} for LMO_2–graphite, where M = Co, Mn...) and insufficient for more demanding applications such as those attending long-range electric vehicles.[1,2] Lithium–sulfur (Li–S) batteries are currently receiving substantial attention, primarily due to their high theoretical capacity of 1675 mAh g^{-1} sulfur (i.e., considering S only) that corresponds to a high gravimetric and volumetric energy density (~2600 Wh kg^{-1} and ~2200 Wh L^{-1}).[1] In addition, sulfur is a naturally abundant element, nontoxic and one of the cheapest energy storage materials.[1,2]

Many technical challenges still attend the Li–S battery involving the cathode, the anode, as well as the electrolyte.[3−10] In general, Li–S batteries suffer from the insulating nature of S and rapid capacity fading occurring as a result of the generation of soluble polysulfide intermediates during discharge.[3,4,8] Polysulfide dissolution gives rise to a shuttle phenomenon that contributes to low Coulombic efficiency and active material loss. The formation of insoluble lithium sulfide (Li_2S) at the end of the discharge process causes a large volume expansion (~80% from S) of the cathode material, which also causes the detachment of active material.[11] Additional concerns facing Li–S batteries include Li dendrite formation and the high reactivity of the Li-metal anode, which results in a nonuniform solid electrolyte interphase (SEI) on the anode surface. This highly resistive passivation film is also associated with performance degradation.[7]

The electrochemical reduction of S_8 results in formation of various polysulfide intermediates through a multistep process. Sulfur speciation has been examined by multiple techniques such as UV–visible absorption spectroscopy (UV–vis),[12,13] X-ray absorption spectroscopy (XAS),[14−16] X-ray diffraction (XRD),[17,18] nuclear magnetic resonance (NMR) and Raman spectroscopy.[19−25] In general, the electrochemical reduction of S_8 normally exhibits two main reduction steps in ionic liquids and organic solvents.[13,26−29] Long chain polysulfides such as Li_2S_8 and Li_2S_6 are produced at the beginning of the discharge process. The long chain polysulfides are reduced to form short chain polysulfides in the further reduction. The final product at the end of discharge is the insoluble lithium sulfide (Li_2S).[3]

Recent reports address structural and morphological changes of the sulfur–carbon cathode during charge and discharge.[18,30−32] In operando transmission X-ray microscopy (TXM) allows tracking of the individual cathode particles in real time during the electrochemical cycling.[18,31] The porosity of the sulfur/super P composite particles increases during the discharge process.[18] In situ X-ray fluorescence microscopy in conjunction with XAS demonstrated the dissolution and redistribution of the sulfur during the first cycle.[32] AFM, HRTEM and Raman spectroscopy showed that part of the polysulfides dissolve into the solution during the reduction process and leave holes in the sulfur–carbon composite matrix. Because of the pronounced morphological change upon the formation of polysulfides, the carbon matrix collapses in part.[30] However, the potential dependence of stability of the sulfur–carbon network is unclear.

Received: July 2, 2015
Accepted: August 28, 2015
Published: August 28, 2015

DOI: 10.1021/acsami.5b05955
ACS Appl. Mater. Interfaces 2015, 7, 20820–20828

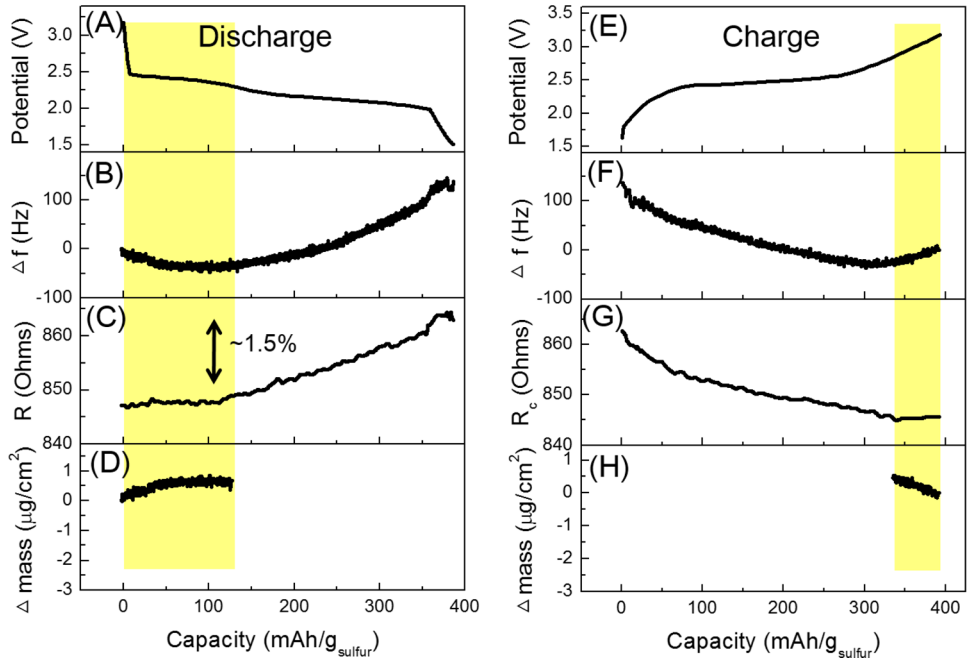

Figure 1. (A–D) In situ EQCM and the discharge profile along with (E–H) in situ EQCM and the charge profile of the sulfur–carbon cathode during the third charge/discharge cycle between 3.2 and 1.5 V at a 1C rate (for the weight of accessed sulfur on the cathode). The yellow band represents the area where ΔR_c is relative small and the Sauerbrey equation is applicable.

Electrochemical quartz crystal microbalance (EQCM) is a gravimetric technique that monitors changes in electrode mass during electrochemical reactions.[33] Substantial prior work using EQCM interrogated reactions occurring on microporous carbon-coated electrode surfaces and Li battery systems such as Li-ion and Li–air batteries has been done.[34−40] For example, in situ EQCM with dissipation[41] was employed to investigate the initial stage of SEI layer formation on cathode-coated Al electrodes for Li-ion battery applications.[35] The observed dissipation change suggested that the rigidity of SEI film decreases with time. The EQCM quantified lithium oxide formation as a function of potential in the Li–O_2 battery.[30] EQCM also explored the irreversible reduction of lithium nitrate, an important additive in Li–S batteries, on bare Au electrodes.[36] However, there is no EQCM study of the sulfur–carbon cathode in Li–S batteries. The EQCM should be capable of monitoring the sulfur–carbon electrode during electrochemical cycling, reporting on changes in mass and structure.

In this work, we used in situ EQCM to examine the sulfur–carbon cathode on the Al-coated quartz crystals during discharge and charge processes in 1 M lithium bis-(trifluoromethane sulfonyl)imide (LiTFSI) and tetraethylene glycol dimethyl ether (TEGDME)/1,3-dioxolane (DOL) (1/1, v/v). As opposed to ordinary EQCM, which relies on the frequency response alone, we also report on the potential and cycle dependence of the crystal resistance (R_c).[42,43] Results are discussed in terms of irreversible changes occurring on the Li–S cathode surface.

2. EXPERIMENTAL SECTION

Sulfur–Carbon Slurry Preparation. The cathode materials were made from a slurry consisting of 60 wt % sulfur (99.98%, Sigma-Aldrich), 30 wt % carbon black (Super-P Li, Timcal Inc.) and 10 wt % polyvinylidene fluoride (PVDF, Kynar 2801) binder mixed with anhydrous *N*-methyl-2-pyrrolidone (NMP, Sigma-Aldrich) and stirred overnight.[22,24]

EQCM Measurements. EQCM measurements were undertaken using a Maxtek RQCM-11000000 (Inficon, USA). QCM crystals were formed from planar, 2.54 cm diameter AT-cut 5 M Hz quartz crystals coated on one side with Al. Prior to use, the Al crystal was rinsed with isopropyl alcohol and sonicated in Milli-Q water for 10 min. After drying, the sulfur–carbon slurry (0.3–0.5 mg) was added dropwise to the Al QCM crystal and dried with Ar again.

The EQCM cell was assembled in an Ar-filled glovebox prior to in situ EQCM measurements as described previously.[38] The sulfur–carbon slurry was the working electrode whereas Li metal (99.9%, Alfa Aesar) formed the reference and counter electrodes. Figure S1 shows a schematic figure of the EQCM cell. The discharge–charge profiles in the EQCM measurement were carried out at a C rate that was calculated by using the weight of the accessed sulfur on the cathode. The accessed sulfur was estimated from the amount of Coulombs during reduction/oxidation process in the CV as compared with the CV obtained from Swagelok cell (Figure S2). EQCM measurements were carried out at 30 °C. All EQCM measurements were carried out by using 760C and 760D CH Instruments potentiostats.

SEM Measurements. The surface morphology of the sulfur–carbon cathode before and after different cycles was analyzed using SEM (JEOL, JSM-7000F). The sulfur–carbon cathodes were cycled in the cycle region between 3.2 and 1.5 V and emersed at 3.2 V. These sulfur–carbon cathodes were then dried in an Ar-filled glovebox overnight and put into a well-sealed container to transfer to the SEM instrument.

Two-Electrode Swagelok-Cell Preparation. The sulfur–carbon slurry was cast on aluminum foil (Sigma-Aldrich) by using a Gardco adjustable micrometer film applicator (Microm 5 1/2 in. width). The sulfur–carbon slurry film was then dried in a convection oven overnight at 55 °C. Lithium–sulfur batteries were assembled in a modified Swagelok tube apparatus. The cell consisted of a Li metal anode, a Whatman glass fiber separator (GF/F, 150 mm diameter) and a sulfur–carbon cathode to which about 0.2 mL of electrolyte was added. Charge and discharge processes in the Swagelok cell were carried out at the rate of 0.1C (calculated using the weight of cathode) by using an Arbin Battery Tester (Model BT 2043, Arbin Instruments Corp., USA).

DOI: 10.1021/acsami.5b05955
ACS Appl. Mater. Interfaces 2015, 7, 20820−20828

Electrolyte. The electrolyte was 1 M lithium bis(trifluoromethane sulfonyl)imide (LiTFSI) in 1:1 (v/v) solution of tetraethylene glycol dimethyl ether (TEGDME, ≥ 99%, Sigma-Aldrich) and 1,3-dioxolane (DOL, anhydrous, Sigma-Aldrich). All EQCM experiments were carried out in the same electrolyte.

3. RESULTS AND DISCUSSION

3.1. In Situ EQCM and Discharge−Charge Process of the Sulfur−Carbon Cathode in TEGDME/DOL Electrolyte. Figure 1A−D shows the results of in situ EQCM measurements and the discharge profile of the as-prepared sulfur−carbon cathode during the third charge/discharge cycle from 3.2 to 1.5 V at a 1C rate. The discharge curve in Figure 1A shows that there are two plateaus around 2.4 and 2.1 V. In our previous in situ Raman spectroscopy studies, the first discharge plateau at ∼2.4 V (marked with the yellow band in Figure 1A−D) is associated with the formation of long chain polysulfides such as Li_2S_8 and Li_2S_6 via opening the S_8 ring during the lithiation process.[24] These long chain polysulfides are further reduced at lower potential. The second discharge plateau at ∼2.1 V is associated with the formation of short chain polysulfides. Li_2S is the final product during the sulfur reduction.[3,12,14] This discharge curve is in good agreement with those in the literature, albeit with somewhat reduced capacity.[3,4,8,24]

To investigate the origin of the reduced capacity seen in the EQCM cell, we constructed a more constrained Li−S battery environment using a Swagelok cell. The capacity obtained from this cell, using an identical C−S slurry, was ∼850 mAh/g sulfur (Figure S3) Thus, the lower capacity obtained from the EQCM measurement is not likely due to the preparation method of the sulfur−carbon cathode, but rather must relate to the substantially larger solvent volume (60 vs 0.2 mL) required for the EQCM.

Figure 1B shows the QCM frequency change obtained from the as-prepared sulfur−carbon cathode during the third discharge process. The frequency decreases gradually in the first plateau region at ∼2.4 V. The frequency starts to increase in the region between 2.4 and 2.0 V, which is associated with the second plateau, and then exhibits a larger increase in the region between 2.0 and 1.5 V. Figure 1B also shows that the measured frequency exhibits a noise level of 10 Hz. In contrast, measurements made with a metallic electrode examining metal deposition typically exhibit a noise level of 0.1 Hz. This suggests that the additional noise is associated with the use of a slurry-based electrode. We found the noise level increased with the thickness of the slurry utilized. Another manifestation of the same phenomena is the increased crystal resistance (R_c) found with the slurry relative to a bare metal electrode (ca. 800 vs 300 Ω). Figure 1C shows the capacity dependence of the R_c measured simultaneously with the change in frequency. R_c is stable during the first discharge plateau, but increases by ca. 1.5% during the second discharge plateau.

The changing R_c behavior shows that different processes are at work on the cathode surface. R_c is low and constant when a purely elastic mass is bound tightly to the surface. However, if the bound mass is inelastic or the dispersion of the surface is not constant, then R_c will change.[44] In this case, the R_c change must be due to increased energy dissipation by the C−S cathode during the second discharge plateau.[44] The change in QCM frequency is usually associated with the change in mass via the Sauerbrey equation. In the limit where ΔR_c is small, the Sauerbrey equation is expected to hold.[33,44] Such is the case in the first discharge plateau. The mass change of the sulfur−carbon cathode in first discharge plateau can be therefore determined by using the Sauerbrey equation:[45]

$$\Delta f = -2\Delta m f^2 / A(\mu\rho_q)^{1/2} = -C_f \Delta m \quad (1)$$

where Δf is the measured resonant frequency (Hz), f is the intrinsic crystal frequency, Δm is the mass change, ρ_q is the density of quartz (2.65 g/cm^3), μ is the shear modulus (2.95×10^{11} dyn/cm^2) and A is the electrode area. In this study, the mass sensitivity factor (C_f) of the carbon cathode was estimated by measuring the frequency change during Ag deposition and stripping on a carbon slurry cathode from a 0.1 M KNO_3 solution containing 1 mM $AgNO_3$ as shown in the Supporting Information (Figure S4). To get C_f from the carbon-coated QCM crystal with a similar R_c, the amount of the coating material (carbon slurry) needs to be well controlled and similar to that used for the Li−S battery work. The slope of the frequency−charge graph can be used to get C_f. The C_f values obtained from bare Al electrodes (53 Hz·cm^2·μg^{-1}) and carbon slurry-coated Al electrodes (50 Hz·cm^2·μg^{-1}) are close. These C_f values are also close to the value obtained from Au QCM crystal (52−57 Hz·cm^2·μg^{-1}) as reported by previous studies.[46,47] Thus, we used a C_f equal to 50 Hz·cm^2·μg^{-1}

Figure 1D shows mass change calculated using the Sauerbrey equation. The increase of Sauerbrey mass in the first discharge plateau is consistent with the occurrence of sulfur lithiation in this region. By the end of the first discharge plateau, the mass increases by ∼0.77 μg/cm^2 at the point where the capacity is ∼130 mAh/g sulfur. On the basis of the charge passed in the first discharge plateau, the expected mass change resulting from sulfur ring opening and lithiation is in a range from 1.2 to 2.4 μg/cm^2, depending on whether only Li_2S_8 is formed (1.2 μg/cm^2) or whether further reduced polysulfides (Li_2S_4) also occur. Our EQCM value is ∼35% lower than the value calculated from the charge when only Li_2S_8 is formed, suggesting that the sulfur−carbon cathode gains mass in the first discharge plateau and ∼35% polysulfide (active material) dissolves into the electrolyte (based on the amount of Li_2S_8) If we assume that Li_2S_4 is formed, our EQCM value would be 38% lower than the calculated value. Interestingly, the capacity we observe at the end of the first plateau (∼130 mAh/g sulfur) represents 65% sulfur available by mass (209 mAh/g sulfur), again suggesting that approximately 35% is lost to dissolution.

We next examine the origin of the frequency change after first discharge plateau in Figure 1B. Figure 1C shows that R_c increases after the first discharge plateau. ΔR_c is related to changes in density (ρ) and viscosity (η) at the electrode surface as first proposed by Muramatsu et al.[48]

$$\Delta R_c = (2\pi f \rho_L \eta_L)^{1/2} A / k^2 \quad (2)$$

where ΔR_c is the resistance change, ρ_L is the density of liquid, η_L is the viscosity of liquid, A is the electrode area and k is an electromechanical factor. The inference from Figure 1C is that the $(\rho_L\eta_L)^{1/2}$ of the product on the surface and sulfur−carbon network is changing because ΔR_c is nonzero, at least in the low voltage discharge region. Thus, the Sauerbrey-mass decrease is due to crystal resistance (R_c) changes and not because of a change in the actual mass. The changing R_c means that the electromechanical properties of the electrode are changing, the origin of which we will discuss below.

Figure 1E−H shows the results of in situ EQCM measurements and the charge profile of the sulfur−carbon

DOI: 10.1021/acsami.5b05955
ACS Appl. Mater. Interfaces 2015, 7, 20820−20828

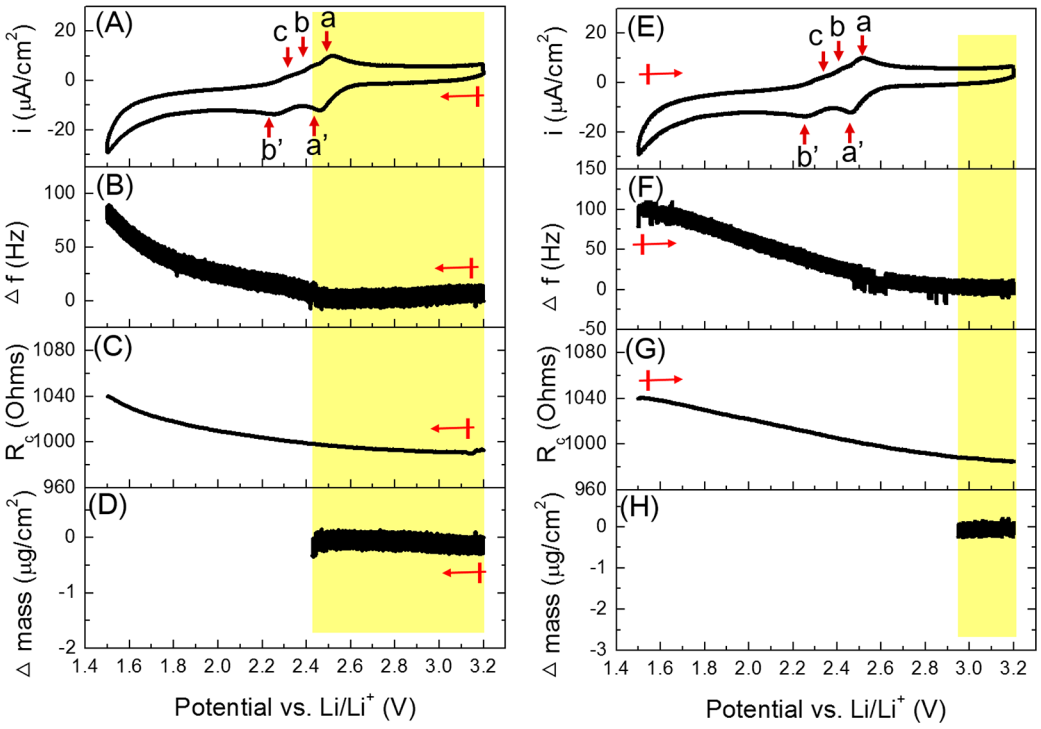

Figure 2. In situ EQCM and third cycle CV profile of the sulfur−carbon cathode during the (A−D) cathodic and (E−H) anodic scan between 3.2 and 1.5 V. The scan rate is 1 mV/s. Red arrows represent the scan direction. The yellow band represent the area where ΔR_c is relatively small and the Sauerbrey equation is applicable.

cathode during the third cycle from 1.5 to 3.2 V at a 1C rate. The yellow band represents the area where the ΔR_c is relatively small and the Sauerbrey equation is applicable. The charge curve in Figure 1E shows a single plateau between 2.35 and 2.5 V that is due to the overlap of two oxidation peaks. These oxidation processes are associated with the oxidation of polysulfides to elemental sulfur during the delithiation process as described in previous work.[14,24]

Figure 1F shows the EQCM frequency change obtained from the sulfur−carbon cathode during the charge process. The frequency decreases in the region between 1.5 and 2.5 V. Coincident with the frequency decrease, R_c also decreases, suggesting the Sauerbrey-mass change is not due to an actual mass change during charge process but rather to a change in the electromechanical properties of the electrode. The frequency then increases in the region of 2.5 to 3.2 V. The relatively constant R_c between 2.6 to 3.2 V suggests that the decrease of Sauerbrey mass is due to the delithiation process in this potential region.

3.2. In Situ EQCM and Cyclic Voltammetry of the Sulfur−Carbon Cathode in TEGDME/DOL Electrolyte. To probe further the gravimetric response of the sulfur−carbon cathode, we performed voltammetric measurements. Figure 2 shows the results of the in situ EQCM measurement along with the CV profile of the sulfur−carbon cathode in a potential range between 3.2 and 1.5 V during the (A−D) cathodic and (E−H) anodic scan. The yellow band represent the area where the ΔR_c is relatively small and the Sauerbrey equation is applicable. Figure 2A shows that the CV starts from the open circuit potential (3.2 V) to 1.5 V. The cathodic scan shows typical sulfur reduction peaks at ∼2.45 V (a′) and ∼2.27 V (b′), respectively. These reduction peaks are associated with the formation of various polysulfides and are correlated with the two discharge plateaus in the discharge profile.[3,11,12,14] In the anodic scan from 1.5 to 3.2 V, there are two oxidative peaks at ∼2.5 V (a) and ∼2.43 V (b) with a small shoulder at ∼2.31 V (c). These peaks are associated with the oxidation of polysulfides to elemental sulfur.[14,24]

Figure 2B shows on the cathodic scan that the frequency is essentially constant in the region between 3.2 and 2.4 V. The constant frequency is associated with both a constant R_c and essentially no mass change from 3.2 to 2.4 V. No change is expected prior to the first reduction peak a′. Following the first reduction peak both the frequency and R_c then increase between 2.4 and 1.5 V, the magnitude of which becomes greater at potentials near 1.5 V. The changing R_c means that the Sauerbrey equation no longer applies in this region. Figure 2E−H shows that both frequency and R_c decrease from 1.5 to 3.2 V in the anodic scan, returning to values close to those obtained before the cathodic scan. Thus, both the CV and the EQCM suggest that reversible processes are occurring in the voltammetry.

3.3. Time Dependent EQCM Measurement of the Sulfur−Carbon Cathode in TEGDME/DOL Electrolyte. To evaluate the stability of the sulfur−carbon electrode under different potential hold conditions, we measured the time dependence of the EQCM frequency and ΔR_c responses. Figure 3A−C shows the time dependent EQCM measurement at 2.4, 2.1, 1.8 and 1.5 V. Figure 3A shows the frequency responses following the different potential steps. The frequency decreases slightly with the time at 2.4 V (after the first reduction peak a′ as shown in Figure 2A) and is constant by the time of a 3 h hold. The small ΔR_c following a step to 2.4 V allows us to calculate the Sauerbrey-mass gain, which is ∼0.25 $\mu g/cm^2$ at this potential. This value is ∼25% less than the value calculated from the charge when only Li_2S_8 is formed.

In contrast to the potential step to 2.4 V, the EQCM frequency increases when the potential was held at either 2.1 or

DOI: 10.1021/acsami.5b05955
ACS Appl. Mater. Interfaces 2015, 7, 20820−20828

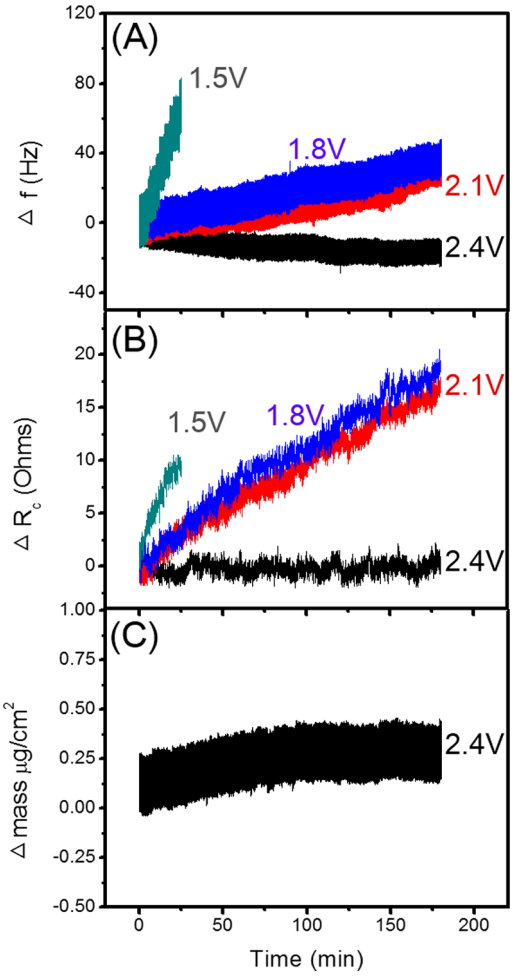

Figure 3. (A–C) Time dependent EQCM measurement of the sulfur–carbon cathode at 2.4, 2.1, 1.8 and 1.5 V.

1.8 V (following the second reduction peak as shown in Figure 2A). Following a potential step to 1.5 V, the frequency increases even more dramatically with time. The frequency changes are also associated with increases in R_c suggesting that properties of the electrode are changing.[42,44,48−53] At 1.5 V, the R_c increase is larger than those found at 2.1 and 1.8 V. Interestingly, neither the frequency nor R_c stabilize during the 3 h time course of the measurement.

We next discuss the origin of the time dependent frequency and R_c increases following potential steps to between 2.1 and 1.5 V. In the model developed by Kanazawa, the frequency change Δf_m arising from a materials property change on the electrode surface is[54,55]

$$\Delta f_m = -f^{3/2}/(\pi\mu\rho_q)^{1/2}[(\rho_1\eta_1)^{1/2} - (\rho_0\eta_0)^{1/2}] \quad (3)$$

Here ρ_0 and η_0 represent the density and viscosity, respectively, of the initial material on the electrode, and ρ_1 and η_1 represent the density and viscosity of the final material. In the present study, we suggest that the observed frequency change Δf is the sum of the frequency change associated with the (de)lithiation process (Δf(de)lithiation) and the change in ($\rho\eta$) during the electrode transformation as it is (de)lithiated (Δf_m):

$$\Delta f = \Delta f_{(de)lithiation} + \Delta f_m \quad (4)$$

Hypothetically, the ($\rho\eta$) of polysulfides could be estimated from R_c at different potential steps, using eq 2.[42,43] Δf_m could then be obtained by using different ($\rho\eta$) of polysulfides at different potential steps. Finally, the actual frequency change due to the (de)lithiation process could be estimated. Unfortunately, R_c does not reach a constant value with time following a potential step to between 2.1 and 1.5 V. This must mean that the electrode is continuously evolving following the potential step and precludes the direct calculation outlined above.

We next outline possible reasons for the R_c development with potential and time. Equation 2 shows that three terms could be responsible for the R_c change: density, viscosity and area. We evaluate each of these in turn. First, the density change going from S_8 to Li_2S (2.07 and 1.66 g/cm^3, respectively) must contribute to the change in R_c during the reduction process. The decrease in density of the material on the cathode during discharge would suggest that R_c should decrease. However, the opposite trend is found experimentally. This must mean that additional factors contribute to R_c evolution.

The second term in eq 2 that could be associated with a change in R_c is the viscosity. Polysulfides formed during discharge could dissolve into the electrolyte and cause an increase in viscosity. Zhang et al. showed that the viscosity of the electrolyte gradually increases with a decrease in the polysulfide chain length and an increase in polysulfide concentration. The viscosity reaches a maximum value at the beginning of the second discharge plateau (~2.0 V).[3] Thus, the viscosity increase before 2.0 V could be associated with the R_c increase. However, our EQCM results show that R_c increases after the first discharge plateau (~2.4 V) and, additionally, exhibits a large increase in the lower potential region, past where the maximum viscosity change occurs. Thus, viscosity change is not the major contributor to the R_c change.

Third, eq 2 shows that R_c depends on the electrode area, A. The increase in R_c with time or potential is likely related to changes in A, (or equivalently electrode roughness) because the other terms in eq 2 are either constant or evolve opposite to the experimental trend, as described above. Previous studies also implicate increases in surface roughness as being associated with increases in R_c. Naoi et al. shows that evolution of a polymer film to a rough or columnar structure leads to a substantial increase in effective surface area causing R_c to increase.[50]

Unrelated to eq 2, other authors suggest that electrode volume might be the origin of a R_c change with a larger change in electrode volume producing a larger ΔR_c.[56] In the Li–S battery, discharge from S_8 to Li_2S leads to a volumetric increase of 79.2% over the entire discharge region. However, the R_c change is only found after the first discharge plateau. Thus, volumetric increase by itself does not seem like a major contribution to R_c change in this work. However, we note that stresses associated with the volume change may result in cracking or other changes that could give rise to an increase in area.

We also address the role of solvent alone in the EQCM response. Figure S5 (Supporting Information) shows in situ EQCM of the bare carbon cathode (without sulfur) in 1 M LiTFSI with TEGDME/DOL. The figure shows that current, frequency, and R_c responses are nominal relative to the dramatic changes occurring when S is included in the cathode.

DOI: 10.1021/acsami.5b05955
ACS Appl. Mater. Interfaces 2015, 7, 20820−20828

Thus, electrolyte insertion does not dominate the EQCM response in our examination of the Li−S system.

On the basis of the discussion above, the increase in the surface area of the sulfur−carbon network is likely the major contributor to the R_c increase after the first discharge plateau. The sulfur−carbon cathode becomes rougher after the first discharge plateau and the roughness increases drastically in the lower potential region. The roughness change may result from short chain polysulfide dissolution after the first discharge plateau and the detachment of Li_2S from the cathode at lower potential region. The sulfur−carbon cathode becomes less rough again from 1.5 to 3.2 V during the charge process. We also found that the roughing process continues over a long time scale.

Our results are consistent with microscopy studies showing that the sulfur−carbon electrode surface evolves with potential, exhibiting much greater porosity and roughness at lower potentials relative to those prior to discharge.[18] We suggest that this roughness increase dominates the QCM response at lower potentials. Interestingly, we find that R_c increases dramatically at 1.5 V relative to an excursion to 1.8 V as shown in Figure 3. We suggest, therefore, that the electrode roughens substantially at this potential, and this evolution raises questions about system reversibility following excursion to 1.5 V, as we describe below.

We next discuss the relationship between Δf and ΔR_c to evaluate further the interaction between the sulfur−carbon cathode network and polysulfides as a function of cycle number (Figure 4). The Δf−ΔR_c plots indicate whether a purely elastic mass binds to the electrode (Δf decreases with ΔR_c = 0) or whether a viscous material (such as the solution) dissipates energy at the surface−liquid interface and effectively adds mass to the electrode (Δf decreases with ΔR_c increase).[44] Figure 4 shows the Δf−ΔR_c diagram of the sulfur−carbon cathode during different discharge−charge cycles between 3.2 and 1.8 V. In the discharge process during the first cycle, Δf decreases with a relatively small ΔR_c until 2.4 V, suggesting the presence of an elastic mass change on the surface. However, past 2.4 V, R_c changes dramatically with Δf (slope = ~0.3 Ω/Hz), a process we previously associated with roughening of the sulfur−carbon electrode. On the reverse scan, during the entire first charging process from 1.8 to 3.2 V, the frequency decreases with the decrease of R_c. The slope is again 0.3 Ω/Hz, which is similar to the first discharge process.

A similar pattern was observed in the second discharge−charge but with a smaller change in Δf between 3.2 and 2.4 V. Interestingly, the Δf−ΔR_c slope is again 0.3 Ω/Hz, suggesting that the same roughening process found during the first cycle occurs again in the second (and subsequent) cycles. A steady state is achieved by the third discharge−charge process.

Figure 4 shows that although the same Δf−ΔR_c slope is found between 2.4 and 1.8 V for all charge−discharge cycles, the Δf−ΔR_c plot is offset with cycle number, suggesting the existence of irreversible processes. To understand the potential dependence of irreversible changes on the sulfur−carbon cathode, we next examine the R_c and frequency offset in different cycle regions. Figure 5A-B shows the frequency and R_c offset obtained after the discharge−charge process cycling between 3.2 and 2.4 V, 3.2 and 1.8 V, and 3.2 and 1.5 V plotted as a function of cycle number. In the cycle region between 3.2 and 1.5 V, the frequency and R_c offset decrease in the first two cycles. The frequency and R_c are relatively stable until reaching ca. 20 charge−discharge cycles, after which the frequency and R_c offset start to increase. In the cycle region between 3.2 and 1.8 V (after second discharge plateau), the frequency and R_c offset decrease in the first two cycles and then are relatively stable until reaching ca. 40 cycles, after which the frequency and R_c offset then increase. In the cycle region between 3.2 and 2.4 V (first discharge plateau), the frequency and R_c offset increase in the first few cycles and are then relatively stable in subsequent cycles.

The decrease in frequency and R_c offset during the first few cycles suggests that an irreversible change occurs in the different cycle regions. This irreversible change in the first few

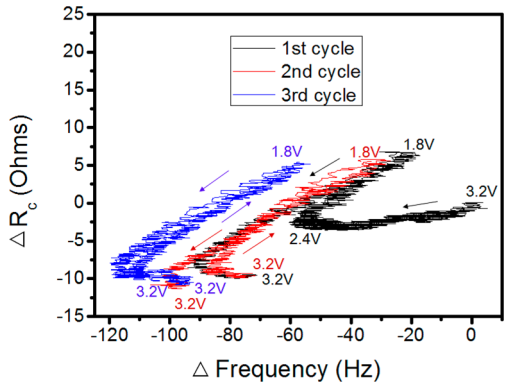

Figure 4. Diagram of frequency change (Δf) and ΔR_c during different discharge−charge cycles between 3.2 and 1.8 V.

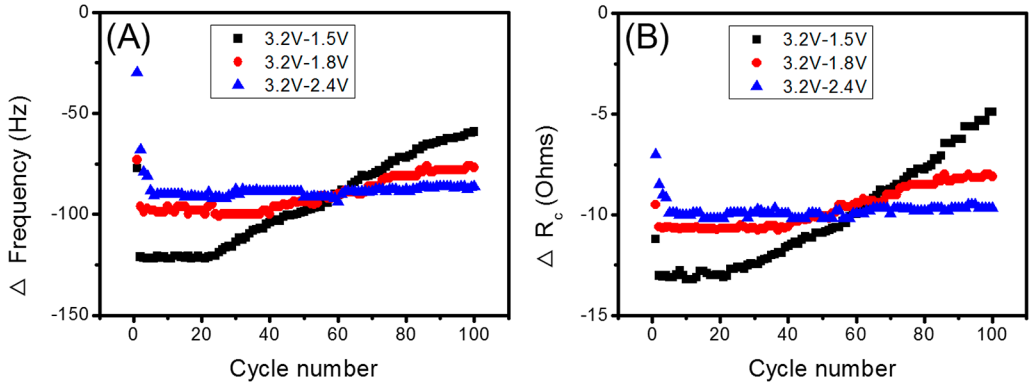

Figure 5. (A,B) Frequency and R_c offset obtained after the discharge−charge process between 3.2 and 2.4, 1.8, 1.5 V were plotted as a function of cycle number.

DOI: 10.1021/acsami.5b05955
ACS Appl. Mater. Interfaces 2015, 7, 20820−20828

cycles may be due to the dissolution of nonaccessed sulfur or the sulfur−carbon network. After the first few cycles, the stable frequency and R_c offset in the cycle region between 3.2 and 2.4 V (first discharge plateau) indicates that the sulfur−carbon electrode is stable during the cycling. The increase in the offset only occurs when the potential was cycled to 1.8 and 1.5 V. As compared with the cycle region between 3.2 and 1.8, and 3.2 and 1.5 V, the larger increase of the offset was found in the cycle region between 3.2 and 1.5 V. This result shows that the sulfur−carbon electrode undergoes irreversible change and becomes rougher during cycling particularly in the cycle region between 3.2 and 1.5 V. The relatively greater stability found cycling between 3.2 and 1.8 V vs 3.2 and 1.5 V suggests that the roughening process is most pronounced with deeper discharge cycles, favoring production of more Li_2S. The increase after ca. 40 cycles suggests the presence of irreversible processes, likely related to continued formation and decomposition of Li_2S during charge and discharge.

We used SEM to visualize the morphology in the sulfur−carbon cathode before cycling and after different charge−discharge cycles. Figure 6 shows SEM images obtained from a

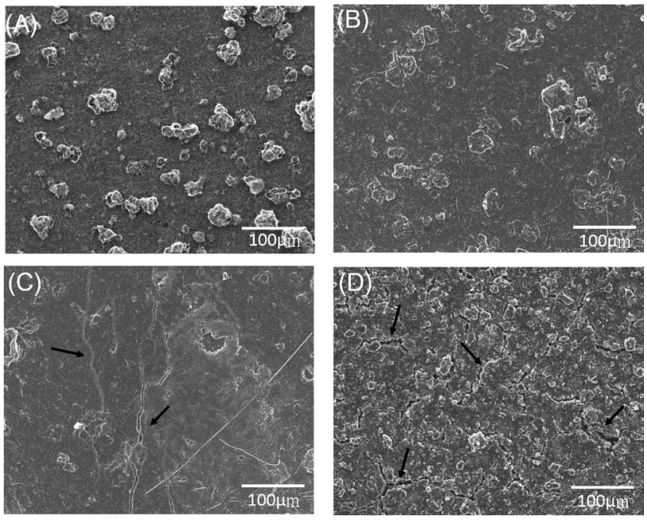

Figure 6. SEM images of the sulfur−carbon cathode (A) before cycle and after (B) 5 cycles, (C) 30 cycles and (D) 100 cycles in the cycle region between 3.2 and 1.5 V. The black arrows indicate the cracks in the sulfur−carbon cathode.

sulfur−carbon cathode before (A) and after (B) 5, (C) 30 and (D) 100 charge−discharge cycles performed between 3.2 and 1.5 V. Figure 6A shows the pristine cathode. The bright areas in Figure 6A are associated with regions of lower electronic conductivity.[57] These bright areas have been previously associated with ∼5−30 μm-sized sulfur-rich particles.[18] EDS results (Figure S6) also exhibit a larger sulfur/carbon ratio in the region of the large particles relative to the bare areas. After five cycles (Figure 6B), the cathode appears fairly uniform, exhibiting particles of ca. 50 μm in extent with some bright areas at edges. After 30 cycles (Figure 6C), SEM images show that the particles are no longer in evidence suggesting that sulfur is more uniformly distributed in the electrode. However, there are a few large cracks apparent, marked with an arrow. In Figure 6D, obtained after 100 charge−discharge cycles, the cracks are more numerous in good agreement with previous studies.[18,30] The development of additional cracking is consistent with the increase in R_c obtained from the EQCM measurements. The cracking may be a consequence the volume change occurring during the formation of Li_2S from S_8.

4. CONCLUSIONS

We used in situ EQCM to evaluate changes in a sulfur−carbon cathodes during charge and discharge. The sulfur−carbon cathode gains mass at the first discharge plateau (∼2.4 V) during the discharge (lithiation) process. Upon further discharge, the increase in R_c suggests that the sulfur−carbon cathode becomes rougher. During the charge (delithiation) process, the roughness of the sulfur−carbon cathode decreases. The $\Delta f-\Delta R_c$ diagram shows the roughening process is dependent on cycle history.

Time dependent measurements show that morphology changes occurring at the sulfur−carbon cathode are small with a shallow discharge (2.4 V) but become large and increase throughout the duration of the measurement with deeper discharge. Irreversible changes in the sulfur−carbon cathode are marked by changes in R_c and increasing frequency offsets with deeper discharge. The sulfur−carbon cathode is stable during the initial cycles, but begins to reflect irreversible changes associated with roughening upon further cycling, changes which are also evidenced by SEM. Volume changes associated with charging and discharging may give rise to the roughening observed.

■ ASSOCIATED CONTENT

Supporting Information

The Supporting Information is available free of charge on the ACS Publications website at DOI: 10.1021/acsami.5b05955.

Schematic figure of the EQCM Cell (Figure S1). CV of the as-prepared sulfur−carbon cathode (∼0.5 mg sulfur/cm^2) in a Swagelok cell (Figure S2). Discharge profiles of Li−S batteries in 1 M LiTFSI with TEGDME/DOL (1:1, by vol) (Figure S3). CV and the Δf response in a solution containing 1 mM $AgNO_3$ and 0.1 M KNO_3 (Figure S4). In situ EQCM and first cycle CV profile of the bare carbon cathode in 1 M LiTFSI with TEGDME/DOL (1:1, by vol) (Figure S5). SEM image and corresponding EDS results from a pristine sulfur−carbon cathode (Figure S6) (PDF).

■ AUTHOR INFORMATION

Corresponding Author

*A. A. Gewirth. E-mail: agewirth@illinois.edu. Telephone: 217-333-8329. Fax: 217-244-5186.

Notes

The authors declare no competing financial interest.

■ ACKNOWLEDGMENTS

This work was supported as part of the Joint Center for Energy Storage Research (JCESR) U.S. Department of Energy Innovation Hub. Funding for JCESR is provided by the U.S. Department of Energy Office of Science.

■ REFERENCES

(1) Bruce, P. G.; Freunberger, S. A.; Hardwick, L. J.; Tarascon, J.-M. Li-O2 and Li-S Batteries with High Energy Storage. *Nat. Mater.* **2011**, *11*, 19−29.

(2) Etacheri, V.; Marom, R.; Elazari, R.; Salitra, G.; Aurbach, D. Challenges in the Development of Advanced Li-ion Batteries: a Review. *Energy Environ. Sci.* **2011**, *4*, 3243−3262.

DOI: 10.1021/acsami.5b05955
ACS Appl. Mater. Interfaces 2015, 7, 20820−20828

(3) Zhang, S. S. Liquid Electrolyte Lithium/Sulfur Battery: Fundamental Chemistry, Problems, and Solutions. *J. Power Sources* **2013**, *231*, 153−162.
(4) Ji, X.; Nazar, L. F. Advances in Li-S batteries. *J. Mater. Chem.* **2010**, *20*, 9821−9826.
(5) Manthiram, A.; Chung, S.-H.; Zu, C. Lithium−Sulfur Batteries: Progress and Prospects. *Adv. Mater.* **2015**, *27*, 1980−2006.
(6) Barghamadi, M.; Best, A. S.; Bhatt, A. I.; Hollenkamp, A. F.; Musameh, M.; Rees, R. J.; Ruther, T. Lithium-Sulfur Batteries-the Solution is in the Electrolyte, but is the Electrolyte a Solution? *Energy Environ. Sci.* **2014**, *7*, 3902−3920.
(7) Cao, R.; Xu, W.; Lv, D.; Xiao, J.; Zhang, J.-G. Anodes for Rechargeable Lithium-Sulfur Batteries. *Adv. Energy Mater.* **2015**, *5*, DOI: 10.1002/aenm.201402273.
(8) Manthiram, A.; Fu, Y.; Chung, S.-H.; Zu, C.; Su, Y.-S. Rechargeable Lithium−Sulfur Batteries. *Chem. Rev.* **2014**, *114*, 11751−11787.
(9) Xu, R.; Lu, J.; Amine, K. Progress in Mechanistic Understanding and Characterization Techniques of Li-S Batteries. *Adv. Energy Mater.* **2015**, *5*, DOI: 10.1002/aenm.201500408.
(10) Scheers, J.; Fantini, S.; Johansson, P. A review of Electrolytes for Lithium−Sulphur Batteries. *J. Power Sources* **2014**, *255*, 204−218.
(11) Nazar, L. F.; Cuisinier, M.; Pang, Q. Lithium-Sulfur Batteries. *MRS Bull.* **2014**, *39*, 436−442.
(12) Barchasz, C.; Molton, F.; Duboc, C.; Leprêtre, J.-C.; Patoux, S.; Alloin, F. Lithium/Sulfur Cell Discharge Mechanism: An Original Approach for Intermediate Species Identification. *Anal. Chem.* **2012**, *84*, 3973−3980.
(13) Han, D.-H.; Kim, B.-S.; Choi, S.-J.; Jung, Y.; Kwak, J.; Park, S.-M. Time-Resolved In Situ Spectroelectrochemical Study on Reduction of Sulfur in N, N ′-Dimethylformamide. *J. Electrochem. Soc.* **2004**, *151*, E283−E290.
(14) Cuisinier, M.; Cabelguen, P.-E.; Evers, S.; He, G.; Kolbeck, M.; Garsuch, A.; Bolin, T.; Balasubramanian, M.; Nazar, L. F. Sulfur Speciation in Li−S Batteries Determined by Operando X-ray Absorption Spectroscopy. *J. Phys. Chem. Lett.* **2013**, *4*, 3227−3232.
(15) Pascal, T. A.; Wujcik, K. H.; Velasco-Velez, J.; Wu, C.; Teran, A. A.; Kapilashrami, M.; Cabana, J.; Guo, J.; Salmeron, M.; Balsara, N.; Prendergast, D. X-ray Absorption Spectra of Dissolved Polysulfides in Lithium−Sulfur Batteries from First-Principles. *J. Phys. Chem. Lett.* **2014**, *5*, 1547−1551.
(16) Wujcik, K. H.; Pascal, T. A.; Pemmaraju, C. D.; Devaux, D.; Stolte, W. C.; Balsara, N. P.; Prendergast, D. Characterization of Polysulfide Radicals Present in an Ether-Based Electrolyte of a Lithium-Sulfur Battery During Initial Discharge Using in Situ X-ray Absorption Spectroscopy Experiments and First-Principles Calculations. *Adv. Energy Mater.* **2015**, *5*, DOI: 10.1002/aenm.201500285.
(17) Walus, S.; Barchasz, C.; Colin, J.-F.; Martin, J.-F.; Elkaim, E.; Lepretre, J.-C.; Alloin, F. New Insight into the Working Mechanism of Lithium-Sulfur Batteries: in situ and Operando X-ray Diffraction Characterization. *Chem. Commun.* **2013**, *49*, 7899−7901.
(18) Nelson, J.; Misra, S.; Yang, Y.; Jackson, A.; Liu, Y.; Wang, H.; Dai, H.; Andrews, J. C.; Cui, Y.; Toney, M. F. In Operando X-ray Diffraction and Transmission X-ray Microscopy of Lithium Sulfur Batteries. *J. Am. Chem. Soc.* **2012**, *134*, 6337−6343.
(19) Huff, L. A.; Rapp, J. L.; Baughman, J. A.; Rinaldi, P. L.; Gewirth, A. A. Identification of Lithium−Sulfur Battery Discharge Products through 6Li and 33S Solid-State MAS and 7Li Solution NMR Spectroscopy. *Surf. Sci.* **2015**, *631*, 295−300.
(20) See, K. A.; Leskes, M.; Griffin, J. M.; Britto, S.; Matthews, P. D.; Emly, A.; Van der Ven, A.; Wright, D. S.; Morris, A. J.; Grey, C. P.; Seshadri, R. Ab Initio Structure Search and in Situ 7Li NMR Studies of Discharge Products in the Li−S Battery System. *J. Am. Chem. Soc.* **2014**, *136*, 16368−16377.
(21) Xiao, J.; Hu, J. Z.; Chen, H.; Vijayakumar, M.; Zheng, J.; Pan, H.; Walter, E. D.; Hu, M.; Deng, X.; Feng, J.; Liaw, B. Y.; Gu, M.; Deng, Z. D.; Lu, D.; Xu, S.; Wang, C.; Liu, J. Following the Transient Reactions in Lithium−Sulfur Batteries Using an In Situ Nuclear Magnetic Resonance Technique. *Nano Lett.* **2015**, *15*, 3309−3316.
(22) Yeon, J.-T.; Jang, J.-Y.; Han, J.-G.; Cho, J.; Lee, K. T.; Choi, N.-S. Raman Spectroscopic and X-ray Diffraction Studies of Sulfur Composite Electrodes during Discharge and Charge. *J. Electrochem. Soc.* **2012**, *159*, A1308−A1314.
(23) Hagen, M.; Schiffels, P.; Hammer, M.; Dörfler, S.; Tübke, J.; Hoffmann, M. J.; Althues, H.; Kaskel, S. In-Situ Raman Investigation of Polysulfide Formation in Li-S Cells. *J. Electrochem. Soc.* **2013**, *160*, A1205−A1214.
(24) Wu, H.-L.; Huff, L. A.; Gewirth, A. A. In Situ Raman Spectroscopy of Sulfur Speciation in Lithium−Sulfur Batteries. *ACS Appl. Mater. Interfaces* **2015**, *7*, 1709−1719.
(25) Chen, J.-J.; Yuan, R.-M.; Feng, J.-M.; Zhang, Q.; Huang, J.-X.; Fu, G.; Zheng, M.-S.; Ren, B.; Dong, Q.-F. Conductive Lewis Base Matrix to Recover the Missing Link of Li2S8 during the Sulfur Redox Cycle in Li−S Battery. *Chem. Mater.* **2015**, *27*, 2048−2055.
(26) Yamin, H.; Gorenshtein, A.; Penciner, J.; Sternberg, Y.; Peled, E. Lithium Sulfur Battery: Oxidation/Reduction Mechanisms of Polysulfides in THF Solutions. *J. Electrochem. Soc.* **1988**, *135*, 1045−1048.
(27) Kim, B. S.; Park, S. M. In Situ Spectroelectrochemical Studies on the Reduction of Sulfur in Dimethyl Sulfoxide Solutions. *J. Electrochem. Soc.* **1993**, *140*, 115−122.
(28) Gaillard, F.; Levillain, E. Visible Time-Resolved Spectroelectrochemistry: Application to Study of the Reduction of Sulfur (S8) in Dimethylformamide. *J. Electroanal. Chem.* **1995**, *398*, 77−87.
(29) Manan, N. S. A.; Aldous, L.; Alias, Y.; Murray, P.; Yellowlees, L. J.; Lagunas, M. C.; Hardacre, C. Electrochemistry of Sulfur and Polysulfides in Ionic Liquids. *J. Phys. Chem. B* **2011**, *115*, 13873−13879.
(30) Elazari, R.; Salitra, G.; Talyosef, Y.; Grinblat, J.; Scordilis-Kelley, C.; Xiao, A.; Affinito, J.; Aurbach, D. Morphological and Structural Studies of Composite Sulfur Electrodes upon Cycling by HRTEM, AFM and Raman Spectroscopy. *J. Electrochem. Soc.* **2010**, *157*, A1131−A1138.
(31) Lin, C.-N.; Chen, W.-C.; Song, Y.-F.; Wang, C.-C.; Tsai, L.-D.; Wu, N.-L. Understanding Dynamics of Polysulfide Dissolution and Redeposition in Working Lithium−Sulfur Battery by In-operando Transmission X-ray Microscopy. *J. Power Sources* **2014**, *263*, 98−103.
(32) Yu, X.; Pan, H.; Zhou, Y.; Northrup, P.; Xiao, J.; Bak, S.; Liu, M.; Nam, K.-W.; Qu, D.; Liu, J.; Wu, T.; Yang, X.-Q. Direct Observation of the Redistribution of Sulfur and Polysufides in Li−S Batteries During the First Cycle by in Situ X-ray Fluorescence Microscopy. *Adv. Energy Mater.* **2015**, *5*, DOI: 10.1002/aenm.201500072.
(33) Buttry, D. A.; Ward, M. D. Measurement of Interfacial Processes at Electrode Surfaces with the Electrochemical Quartz Crystal Microbalance. *Chem. Rev.* **1992**, *92*, 1355−1379.
(34) Sharon, D.; Etacheri, V.; Garsuch, A.; Afri, M.; Frimer, A. A.; Aurbach, D. On the Challenge of Electrolyte Solutions for Li−Air Batteries: Monitoring Oxygen Reduction and Related Reactions in Polyether Solutions by Spectroscopy and EQCM. *J. Phys. Chem. Lett.* **2013**, *4*, 127−131.
(35) Yang, Z.; Ingram, B. J.; Trahey, L. Interfacial Studies of Li-Ion Battery Cathodes Using In Situ Electrochemical Quartz Microbalance with Dissipation. *J. Electrochem. Soc.* **2014**, *161*, A1127−A1131.
(36) Rosenman, A.; Elazari, R.; Salitra, G.; Markevich, E.; Aurbach, D.; Garsuch, A. The Effect of Interactions and Reduction Products of LiNO3, the Anti-Shuttle Agent, in Li-S Battery Systems. *J. Electrochem. Soc.* **2015**, *162*, A470−A473.
(37) Aurbach, D.; Zaban, A. The Application of EQCM to the Study of the Electrochemical Behavior of Propylene Carbonate Solutions. *J. Electroanal. Chem.* **1995**, *393*, 43−53.
(38) Tavassol, H.; Buthker, J. W.; Ferguson, G. A.; Curtiss, L. A.; Gewirth, A. A. Solvent Oligomerization during SEI Formation on Model Systems for Li-Ion Battery Anodes. *J. Electrochem. Soc.* **2012**, *159*, A730−A738.
(39) Levi, M. D.; Salitra, G.; Levy, N.; Aurbach, D.; Maier, J. Application of a Quartz-Crystal Microbalance to Measure Ionic Fluxes in Microporous Carbons for Energy Storage. *Nat. Mater.* **2009**, *8*, 872−875.

DOI: 10.1021/acsami.5b05955
ACS Appl. Mater. Interfaces 2015, 7, 20820−20828

(40) Yang, Z.; Gewirth, A. A.; Trahey, L. Investigation of Fluoroethylene Carbonate Effects on Tin-based Lithium-Ion Battery Electrodes. *ACS Appl. Mater. Interfaces* **2015**, *7*, 6557−6566.
(41) Reviakine, I.; Johannsmann, D.; Richter, R. P. Hearing What You Cannot See and Visualizing What You Hear: Interpreting Quartz Crystal Microbalance Data from Solvated Interfaces. *Anal. Chem.* **2011**, *83*, 8838−8848.
(42) Serizawa, N.; Seki, S.; Takei, K.; Miyashiro, H.; Yoshida, K.; Ueno, K.; Tachikawa, N.; Dokko, K.; Katayama, Y.; Watanabe, M.; Miura, T. EQCM Measurement of Deposition and Dissolution of Lithium in Glyme-Li Salt Molten Complex. *J. Electrochem. Soc.* **2013**, *160*, A1529−A1533.
(43) Serizawa, N.; Katayama, Y.; Miura, T. EQCM Measurement of Ag (I)/Ag Reaction in an Amide-Type Room-Temperature Ionic Liquid. *J. Electrochem. Soc.* **2009**, *156*, D503−D507.
(44) Marx, K. A. Quartz Crystal Microbalance: A Useful Tool for Studying Thin Polymer Films and Complex Biomolecular Systems at the Solution−Surface Interface. *Biomacromolecules* **2003**, *4*, 1099−1120.
(45) Sauerbrey, G. Verwendung von Schwingquarzen zur Wägung dünner Schichten und zur Mikrowägung. *Eur. Phys. J. A* **1959**, *155*, 206−222.
(46) Uchida, H.; Hiei, M.; Watanabe, M. Electrochemical Quartz Crystal Microbalance Study of Copper Adatoms on Au(111) Electrodes in Solutions of Perchloric and Sulfuric Acid. *J. Electroanal. Chem.* **1998**, *452*, 97−106.
(47) Tsai, W.-Y.; Taberna, P.-L.; Simon, P. Electrochemical Quartz Crystal Microbalance (EQCM) Study of Ion Dynamics in Nanoporous Carbons. *J. Am. Chem. Soc.* **2014**, *136*, 8722−8728.
(48) Muramatsu, H.; Tamiya, E.; Karube, I. Computation of Equivalent Circuit Parameters of Quartz Crystals in Contact with Liquids and Study of Liquid Properties. *Anal. Chem.* **1988**, *60*, 2142−2146.
(49) Muramatsu, H.; Egawa, A.; Ataka, T. Reliability of Correlation Between Mass Change and Resonant Frequency Change for a Viscoelastic-Film-Coated Quartz Crystal. *J. Electroanal. Chem.* **1995**, *388*, 89−92.
(50) Naoi, K.; Oura, Y.; Maeda, M.; Nakamura, S. Electrochemistry of Surfactant-Doped Polypyrrole Film(I): Formation of Columnar Structure by Electropolymerization. *J. Electrochem. Soc.* **1995**, *142*, 417−422.
(51) Topart, P. A.; Noel, M. A. M. High-Frequency Impedance Analysis of Quartz Crystal Microbalances. 2. Electrochemical Deposition and Redox Switching of Conducting Polymers. *Anal. Chem.* **1994**, *66*, 2926−2934.
(52) Bund, A.; Schneider, O.; Dehnke, V. Combining AFM and EQCM for the in situ Investigation of Surface Roughness Effects during Electrochemical Metal Depositions. *Phys. Chem. Chem. Phys.* **2002**, *4*, 3552−3554.
(53) Etchenique, R. A.; Calvo, E. J. Gravimetric Measurement in Redox Polymer Electrodes with the EQCM Beyond the Sauerbrey Limit. *Electrochem. Commun.* **1999**, *1*, 167−170.
(54) Kanazawa, K. K.; Gordon, J. G. Frequency of a Quartz Microbalance in Contact with Liquid. *Anal. Chem.* **1985**, *57*, 1770−1771.
(55) Lee, W. W.; White, H. S.; Ward, M. D. Depletion Layer Effects on the Response of the Electrochemical Quartz Crystal Microbalance. *Anal. Chem.* **1993**, *65*, 3232−3237.
(56) Severin, E. J.; Lewis, N. S. Relationships among Resonant Frequency Changes on a Coated Quartz Crystal Microbalance, Thickness Changes, and Resistance Responses of Polymer−Carbon Black Composite Chemiresistors. *Anal. Chem.* **2000**, *72*, 2008−2015.
(57) Devaney, J. R.; Leedy, K. O.; Keery, W. *Notes on SEM Examination of Microelectronic Devices*; U.S. Department of Commerce, National Bureau of Standards: Gaithersburg, MD, 1977.

DOI: 10.1021/acsami.5b05955
ACS Appl. Mater. Interfaces 2015, 7, 20820−20828